SINTEF
PROCEEDINGS
1

Selected papers from 10th International Conference on Computational Fluid Dynamics in the Oil & Gas, Metallurgical and Process Industries

# Progress in Applied CFD

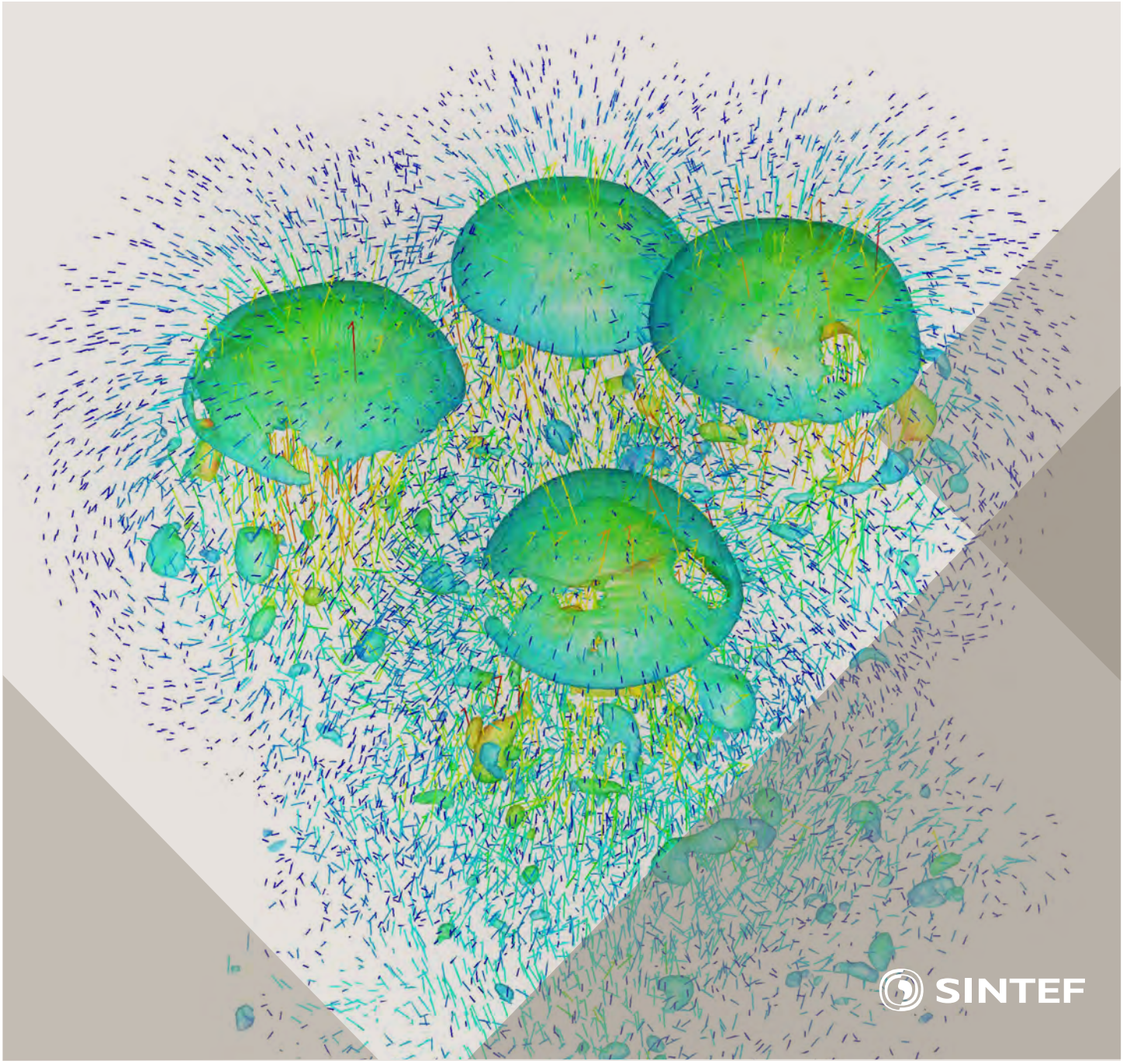

SINTEF Proceedings

Editors:
Jan Erik Olsen and Stein Tore Johansen

# Progress in Applied CFD

Selected papers from 10th International Conference on Computational Fluid Dynamics in the Oil & Gas, Metallurgical and Process Industries

SINTEF Academic Press

SINTEF Proceedings no 1
Editors: Jan Erik Olsen and Stein Tore Johansen
**Progress in Applied CFD**
Selected papers from 10th International Conference on Computational Fluid Dynamics in the Oil & Gas, Metallurgical and Process Industries

Key words:
CFD, Flow, Modelling

Cover, illustration: Rising bubbles by Schalk Cloete

ISSN 2387-4287 (printed)
ISSN 2387-4295 (online)
ISBN 978-82-536-1432-8 (printed)
ISBN 978-82-536-1433-5 (pdf)

60 copies printed by AIT AS e-dit
Content: 100 g munken polar
Cover: 240 g trucard



SINTEF Academic Press
Address: Forskningsveien 3 B
PO Box 124 Blindern
N-0314 OSLO
Tel: +47 22 96 55 55
Fax: +47 22 96 55 08

www.sintef.no/byggforsk
www.sintefbok.no

**SINTEF Proceedings**
SINTEF Proceedings is a serial publication for peer-reviewed conference proceedings on a variety of scientific topics.
The processes of peer-reviewing of papers published in SINTEF Proceedings are administered by the conference organizers and proceedings editors. Detailed procedures will vary according to custom and practice in each scientific community.

## PREFACE

This book contains selected papers from the 10th International Conference on Computational Fluid Dynamics in the Oil & Gas, Metallurgical and Process Industries. The conference was hosted by SINTEF in Trondheim in June 2014 and is also known as CFD2014 for short. The conference series was initiated by CSIRO and Phil Schwarz in 1997. So far the conference has been alternating between CSIRO in Melbourne and SINTEF in Trondheim. The conferences focus on the application of CFD in the oil and gas industries, metal production, mineral processing, power generation, chemicals and other process industries. The papers in the conference proceedings and this book demonstrate the current progress in applied CFD.

The conference papers undergo a review process involving two experts. Only papers accepted by the reviewers are presented in the conference proceedings. More than 100 papers were presented at the conference. Of these papers, 27 were chosen for this book and reviewed once more before being approved. These are well received papers fitting the scope of the book which has a slightly more focused scope than the conference. As many other good papers were presented at the conference, the interested reader is also encouraged to study the proceedings of the conference.

The organizing committee would like to thank everyone who has helped with paper review, those who promoted the conference and all authors who have submitted scientific contributions. We are also grateful for the support from the conference sponsors: FACE (the multiphase flow assurance centre), Total, ANSYS, CD-Adapco, Ascomp, Statoil and Elkem.

Stein Tore Johansen & Jan Erik Olsen

Organizing committee:

Conference chairman: Prof. Stein Tore Johansen
Conference coordinator: Dr. Jan Erik Olsen
Dr. Kristian Etienne Einarsrud
Dr. Shahriar Amini
Dr. Ernst Meese
Dr. Paal Skjetne
Dr. Martin Larsson
Dr. Peter Witt, CSIRO

Scientific committee:

J.A.M.Kuipers, TU Eindhoven
Olivier Simonin, IMFT/INP Toulouse
Akio Tomiyama, Kobe University
Sanjoy Banerjee, City College of New York
Phil Schwarz, CSIRO
Harald Laux, Osram
Josip Zoric, SINTEF
Jos Derksen, University of Aberdeen
Dieter Bothe, TU Darmstadt
Dmitry Eskin, Schlumberger
Djamel Lakehal, ASCOMP
Pär Jonsson, KTH
Ruben Shulkes, Statoil
Chris Thompson, Cranfield University
Jinghai Li, Chinese Academy of Science
Stefan Pirker, Johannes Kepler Univ.
Bernhard Müller, NTNU
Stein Tore Johansen, SINTEF
Markus Braun, ANSYS

## CONTENTS

# NUMERICAL MODEL FOR FLOW IN ROCKS COMPOSED OF MATERIALS OF DIFFERENT PERMEABILITY

**R.R. LI[2], Y.S. YANG[1], J. PAN[2], G.G. PEREIRA[1*] ,J.A. TAYLOR[3], M.B. CLENNELL[4], C. ZOU[5]**

[1] CSIRO, Private Bag 33, Clayton 3169, AUSTRALIA

[2] North University of China, School of Information and Communication Engineering, Shanxi, 030051, CHINA

[3]CSIRO, G.P.O. Box 664, Canberra, 2601, AUSTRALIA

[4]CSIRO, P.O. Box 1130, Bentley, 6102, AUSTRALIA

[5]Research Institute of Petroleum Exploration and Development (RIPED), PetroChina, Beijing, CHINA

* E-mail: Gerald.Pereira@csiro.au

## ABSTRACT

In the oil and gas industry permeability measurements on rock samples give an indication of the capacity to produce the output (oil/gas etc). Permeability of small samples can be derived from x-ray Computed Tomography (CT) scans which yields a three-dimensional (binary) digital image of the sample. Then using suitable numerical tools, one can use this digital data to compute a velocity field and hence the permeability of the sample. Up to now, this has been done on the assumption that fluid can only flow in pores (with no flow in solid regions). However, if the sample is made up of different materials, each material can have a different permeability to fluid flow. Hence, here we consider numerical modelling of flow through such a material. We use the Lattice Boltzmann method to model this flow, but need to change the usual streaming and collision steps to account for the partial permeability of voxels. We first implement this new algorithm on some well-known test cases, with excellent agreement with analytic results and then use our algorithm on some real CT digital data. Our results clearly show the effect of increasing the local fraction of a high permeability material within a sample on the global permeability.

**Keywords:** Lattice Boltzmann, Computed Tomography scan, digital data, partial permeability.

## NOMENCLATURE

*Greek Symbols*

$\rho$ LB particle density, [dimensionless].
$\mu$ LB dynamic viscosity, [dimensionless].
$\nu$ LB kinematic viscosity, [dimensionless].

*Latin Symbols*

$n_s$ solid fraction, [dimensionless].
$p_f$ percolating fraction, [dimensionless].
$P$ LB Pressure, [dimensionless].
$f$ LB particle distribution function, [dimensionless].
$\boldsymbol{u}$ LB Velocity, [dimensionless].
$c_s$ LB speed of sound, [dimensionless].
$K$ LB Permeability [dimensionless].

*Sub/superscripts*

$\alpha$ LB velocity direction.
$x$ Index $x$ – Cartesian axis.
$y$ Index $y$ – Cartesian axis.
$z$ Index $z$ – Cartesian axis.

## INTRODUCTION

Fluid flow in porous media is widely encountered in oil and gas development and production, in addition to various other physical and chemical processes. The Lattice Boltzmann model (LBM) has recently attracted considerable attention in fluid flow simulations in porous media. However, LBM simulations often require an explicit and discrete description of the underlying pore-space geometry. For some applications, such as with unconventional oil and gas reservoirs, the pore sizes encompassing length scales from the nm to mm are relevant. It is technically unfeasible to characterize the pores across such multiple length scales, and computationally unpractical to simulate fluid flow on them with the traditional LBM. As an alternative approach, a partial-bounce-back LBM was suggested by Dardis and McCloskey (1998a, 1998b), which is a meso-scale LBM approach that incorporates the permeability of the medium as a model parameter. Multiple neighboring voxels could be grouped together to form nodes. The LBM simulations were performed on a lattice consisting of such nodes. Rather than a lattice comprising nodes that are either solid or fluid, this is a probabilistic model, where lattice node properties are varied to reflect the local permeability of the material. Their model was inspired by earlier work with lattice gases in which variable permeability materials were simulated by introducing random scatters into the lattice (Balasubramanian *et al.*, 1987; Gao and Sharma, 1994). However, Dardis and McCloskey's (1992a, 1992b) Lattice Boltzmann approach avoided the statistical noise that is inherent in lattice gas models. To date, several different possible models have been proposed for formulating partial-bounce-back LBM approach, described in (Thorne and Sukop, 2004; Walsh *et al.*, 2009; Zhu and Ma, 2013). In all these models, a key parameter $n_s$, referred to as solid

fraction, is used. It is worth noting that the solid fraction should be regarded as an internal model parameter related to the permeability, rather than a reflection of the actual proportion of solid material at each node. An analytic expression that relates the permeability to solid fraction was derived by Walsh *et al.* (2009). As will be discussed in the next section, an effective percolating fraction $p_f$ (equivalent to 1-$n_s$) would be a more appropriate notation.

For the existing partial-bounce-back LBM approach, it is required to determine $n_s$ at every lattice node. The discrete internal structure of a node may be characterized approximately using X-ray CT together with an image segmentation method by Desrues *et al* (2006). The permeability of the node is calculated based on its internal structure. When the local permeability of a node was known, and it was homogeneous and isotropic, $n_s$ for the node could be estimated using the equation given in Walsh *et al* (2009). A procedure for estimating the model parameter $n_s$ is proposed in Zhu and Ma (2013). However, a typical sample may contain too many lattice nodes for this to work in practice. Even if the local permeability is estimated at a limited set of selected locations only, it is a non-trivial task to extrapolate them to other locations to obtain all the required $n_s$ values.

It is worth noting that the existing LBM approaches are modeled on binary voxels. That is, a voxel is occupied by either solid or void. If a voxel is partial solid or void, the existing LBM is not applicable. Recently, a data-constrained modeling (DCM) approach has been developed which can generate microscopic partial volume distributions of materials and pores, therefore incorporating the effects of the fine length scale below X-ray CT resolution (Yang *et al*, 2007, Yang *et al*, 2008). In the model, each voxel was represented by partial volumes of various different materials rather than the binary value of only one material present in traditional image segmentation.

In this paper, the partial-bounce-back LBM approach is combined with the DCM partial volume model to simulate fluid flow in porous materials. The partial-bounce-back LBM is extended to incorporate such partial volume voxels at the microscopic length scale on a regular lattice. This enables more accurate permeability simulations for macroscopic samples with fine structures below voxel resolution. The effective percolating fraction $p_f$ introduced in the advanced partial-bounce-back LBM is non-constant through the porous medium. The percolating fraction can be estimated using the volume fractions of the voxels. The advanced approach has been applied to simulate flow between parallel walls and in rectangular duct flow in 2D and 3D respectively. The permeability of two real world sandstone samples is also calculated with the presented method.

Note that we use a single relaxation time (SRT) implementation of the LBM method in this study. However, it is well known (Pereira *et al.*, 2012) that the permeability obtained from an SRT scheme is viscosity dependent. As such, to obtain viscosity independent results, one should use a multi-relaxation time (MRT) scheme. Since we are only demonstrating the feasibility of a new partial bounce-back approach, we implement the simpler SRT scheme in this paper and leave a full MRT scheme to future work.

## MODEL DESCRIPTION

### Partial-bounce-back Lattice Boltzmann model

The Lattice Boltzmann model is a numerical technique for modeling fluid dynamics. The fluid is represented by discrete fluid particles, with a given mass and velocity, which propagate on a lattice. At each time-step in traditional LBM method, the fluid particles undergo a two-step process:

(1) Streaming step: In this step, the fluid particles are propagated between neighboring nodes. Streaming should be treated as an intermediate step. The result after streaming is denoted by $f^*_\alpha$:

$$f_\alpha^*(\mathbf{x}+\mathbf{e}_\alpha\Delta t,t) = f_\alpha(\mathbf{x},t), \qquad (1)$$

where, $f_\alpha(\mathbf{x},t)$ is the particle distribution function in the direction $\alpha$, $\mathbf{x}$ is the centre coordinate of a lattice node and $t$ is time, while $\Delta t$ is the time increment. $\mathbf{e}_\alpha$ is the unit velocity vector in direction $\alpha$. In this study, the two-dimensional 9-velocity (D2Q9) and three-dimensional 19-velocity (D3Q19) lattice Boltzmann models were used. That is, the direction $\alpha$ takes 9 and 19 discrete *values* respectively (which include the null vector).

(2) Collision step: In this step, the fluid particles, converging on individual nodes, are redistributed according to a set of predefined rules. Which rule is applied in the collision step depends on whether the node is part of the fluid domain or part of the solid-fluid boundary.

(I) If the node represents part of the fluid domain, then the evolution equation is

$$f_\alpha(\mathbf{x},t+\Delta t) = f_\alpha^*(\mathbf{x},t) + [f_\alpha^{eq}(\mathbf{x},t) - f_\alpha^*(\mathbf{x},t)]/\tau, \quad (2)$$

where, $\tau$ is the dimensionless relaxation time. In this study $\tau$ is taken to be one. $f_\alpha^{eq}(\mathbf{x},t)$ are the equilibrium distribution functions and selected according to a Maxwell distribution.

(II) If a lattice node is part of a solid-fluid boundary with no-slip conditions, then the fluid particles undergo a bounce-back boundary condition. As the name suggests, at these nodes, the incoming fluid particles are reflected in the opposite direction during the collision step. $\alpha'$ is the opposite direction of $\alpha$:

$$f_\alpha(\mathbf{x},t+\Delta t) = f_{\alpha'}^*(\mathbf{x},t) \ . \qquad (3)$$

For porous media, the collision step (I) would be considered as a second intermediate step after streaming, and the partial-bounce-back method and collision step (II) were both incorporated into the third process, referred to as porous media step. Denoting $f_\alpha^{**}$ as the result of the collision step (I), at each time-step the fluid particles undergo a three-step process:

(1) streaming step:

$$f_\alpha^*(\mathbf{x}+\mathbf{e}_\alpha\Delta t,t)=f_\alpha(\mathbf{x},t)\ , \qquad (4)$$

(2) collision step:

$$f_\alpha^{**}(\mathbf{x},t+\Delta t)=f_\alpha^*(\mathbf{x},t)+[f_\alpha^{eq}(\mathbf{x},t)-f_\alpha^*(\mathbf{x},t)]/\tau\ , \qquad (5)$$

(3) porous media step:

$$f_\alpha(\mathbf{x},t+\Delta t)=f_\alpha^{**}(\mathbf{x},t+\Delta t)+n_s\cdot\Delta f\ , \qquad (6)$$

where, $n_s(\mathbf{x})$ is the solid fraction mentioned previously per lattice node $\mathbf{x}$. The density per node $\rho$ and the macroscopic flow velocity $\boldsymbol{u}$ are defined in terms of the particle distribution function by (the D2Q9 model)

$$\sum_{\alpha=0}^{8} f_\alpha=\rho\ ,\ \sum_{\alpha=0}^{8} f_\alpha\,\mathbf{e}_\alpha=\rho\,\mathbf{u}\ , \qquad (7)$$

where the pressure is given by $P = c_s^2\rho$, and $c_s$ is the speed of sound with $c_s^2=1/3$.

According to different partially bounce-back models, the term $\Delta f$ has various forms. The following are three common forms:

(I) first form:

$$\Delta f = f_{\alpha'}(\mathbf{x},t)-f_\alpha(\mathbf{x}-\mathbf{e}_\alpha\Delta t,t)\ . \qquad (8)$$

This form was proposed by Dardis and McCloskey (1998).

(II) second form:

$$\Delta f = f_{\alpha'}^{**}(\mathbf{x}+\mathbf{e}_\alpha\Delta t,t+\Delta t)-f_\alpha^{**}(\mathbf{x},t+\Delta t)\ . \qquad (9)$$

This form was proposed by Thorne and Sukop (2004).

(III) third form:

$$\Delta f = f_{\alpha'}^{*}(\mathbf{x},t)-f_\alpha^{**}(\mathbf{x},t+\Delta t)\ . \qquad (10)$$

This form is proposed by Walsh *et al* (2009). It was demonstrated in this paper that only the third form can conserve mass in heterogeneous media.

### Partially percolating Lattice Boltzmann model

In order to incorporate the partial volume effect into the traditional partial-bounce-back LBM, an effective percolating fraction $p_f$ for each voxel is introduced to replace the solid fraction $n_s$. In the above, the first and second forms both use data from the neighbouring nodes to calculate the term $\Delta f$. This would create complications for parallel computation implementation. Significant data exchange and synchronization would be required between processors at each time-step. The third model has the advantage that the collision and porous media step are performed simultaneously without referring to neighbouring nodes. In the following, the third form was used which was named as partially-percolating Lattice Boltzmann model (PP-LBM).

Similar to the LBM approach for porous media, at each time-step in PP-LBM the fluid particles undergo a three-step process: streaming, collision, and porous media steps. The third step could be expressed as:

$$f_\alpha(\mathbf{x},t+\Delta t)=f_\alpha^{**}(\mathbf{x},t+\Delta t)+\left[1-p_f(\mathbf{x})\right]\cdot[f_{\alpha'}^{*}(\mathbf{x},t)-f_\alpha^{**}(\mathbf{x},t+\Delta t)]\ . \qquad (11)$$

## SIMULATIONS IN REGULAR GEOMETRIES

### Flow between parallel walls

With an incompressible fluid, Poiseuille flow is created between stationary parallel walls (which forms a channel) when a constant pressure difference $\Delta P$ is applied between the two openings at the end of the walls. The velocity distribution can be solved analytically. It is parabolic and is given by

$$u(y)=\frac{G\cdot(L-y)\cdot y}{2\mu}\ , \qquad (12)$$

where $G$ is a constant pressure gradient, $\mu$ is the dynamic viscosity, $L$ is the perpendicular separation between the two parallel walls so that fluid flows in the channel between $0\le y\le L$.

In order to evaluate the accuracy of the PP-LBM approach as described in Equations (4), (5) and (11), the flow is simulated numerically on a $51\times101$ square lattice with a D2Q9 model, where $0\le x\le 50$, $0\le y\le 100$, using pressure boundary conditions at the inlet and outlet. To model the impermeable walls, where we have a no slip boundary condition, we simply use $p_f = 0$. The lattice sites between the two walls were assigned the value $p_f = 1$. That is, it is fully void between the walls. For numerical convenience, the simulations were carried out using LBM units where the fluid density is $\rho = 1$, and the dynamic viscosity $\mu = 1/6$. The flow was driven by a constant pressure difference between the inlet and outlet of the flow region, which is generated using a pressure boundary condition in 2D (Zou and He, 1997, Hecht and Harting, 2010). The pressure difference is expressed as $\Delta P=c_s^2\,(\rho_{in}-\rho_{out})$, $\rho_{in}$ is the density of nodes at the inlet with $\rho_{in}=1.00001$ and $\rho_{out}$ is the density of nodes at the outlet with $\rho_{out} = 0.99999$. The value of the pressure difference is $\Delta P = 0.67 \times 10^{-5}$. A relationship between Reynolds number and pressure difference $\mathrm{Re}=\sqrt{(\Delta P/\Delta x)\cdot L^3\cdot\rho}/\mu$ is used to relate the LBM units to physical units. For a fluid with a density $\rho = 10^3$ kg/m$^3$ and a dynamic viscosity $\mu = 10^{-3}\,\mathrm{kg/m\cdot s}$, the value of constant pressure difference is $\Delta P = 1.5 \times 10^{-5}$ Pa. When the flow reaches a steady-state, the fluid speed depends only on $y$. The simulation results and the analytic solution are shown in Figure 1. The figure shows an excellent agreement between the analytical solution and the PP-PBM numerical results.

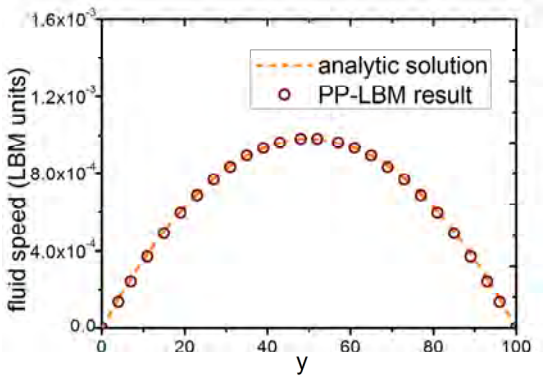


**Figure 1.** PP-LBM simulation of flow between parallel walls. Analytical solution from Eq. (12) is shown as solid lines and the PP-LBM numerical results at $x$=25 are shown as circles.

When pixels between the two non-percolating walls are partially percolating with $p_f$ < 1, the fluid velocity distribution is quite different. This problem can also be solved analytically (Balasubramanian, 1987). The solution is expressed as

$$u(y) = -\frac{G}{\varphi\rho}[1-\frac{\cosh[r(y-L/2)]}{\cosh(r\cdot L/2)}] \ , \qquad (13)$$

where $\varphi$ is a damping coefficient proportional to 1-$p_f$. $\varphi$ and $r$ are related through $r=\sqrt{\varphi/\nu}$ and $\nu=\mu/\rho$ is the kinematic viscosity. As $\varphi \to 0$, the solution (13) returns to the standard Poiseuille equation. As additional verifications of the PP-LBM approach, various uniform values of the effective percolating fraction $p_f$ between the non-percolating walls have been simulated from 0.01 to 0.9. Again, the steady-state flow speed depends only on *y*. The simulated speed distributions (symbols) for various uniform values $p_f$, as a function of *y*, are shown in Figure 2. The analytic results (continuous curves) are also included in Figure 2. Excellent agreement has been obtained between the PP-LBM numerical simulations and analytic solutions. In addition, our numerical results show no abnormal behaviour for all values of $p_f$ in (0, 1). In contrast, the model by Dardis and McCloskey has produced obvious errors near the boundaries for $p_f$ < 0.7 (Chen and Zhu, 2008).

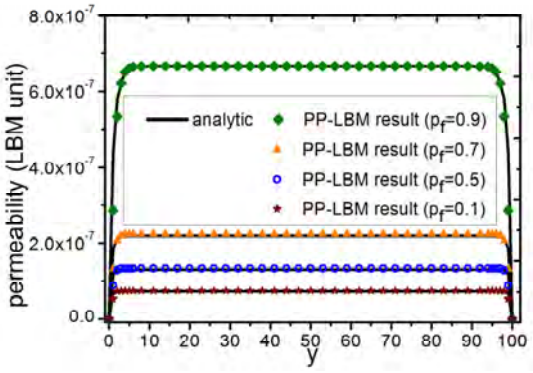


**Figure 2.** Simulation results when the percolating fraction changed. Analytical solutions from Eq. (13) are shown as solid lines and the PP-LBM numerical results at x=25 are shown as markers.

## Flow in a rectangular duct

For a duct with a rectangular cross section, the same pressure difference $\Delta P$ creates a quasi-parabolic velocity distribution when the effective percolating fraction is $p_f$ = 1. It can be calculated that the product of the friction coefficient $f$ (a dimensionless variable which quantifies the overall viscous drag) and the Reynolds number Re is a constant. This quantity is given by (Tao and Xu, 2001)

$$f\cdot \mathrm{Re} = \frac{2\cdot\Delta P\cdot de^2}{\mu\cdot L_z\cdot\bar{u}}, \qquad de=\frac{4\cdot L_x\cdot L_y}{2(L_x+L_y)} \ , \ (14)$$

where $L_z$ is the duct length along the *z* axis in the flowing direction, $L_x$, and $L_y$ are the duct widths in the *x* and *y* directions respectively. $\bar{u}$ is the average velocity of a cross section.

As another validation of the PP-LBM approach, a numerical simulation was implemented on a 101 x 101 x 51 simple cubic lattice with a D3Q19 model, where $0 \le x \le 100$, $0 \le y \le 100$, $0 \le z \le 50$. To model the four impermeable walls, where we have a no-slip boundary condition, we simply use $p_f$ = 0. The lattice sites in the rectangular flow region were assigned the value $p_f$ = 1. The flow is driven by the same pressure difference as the 2D simulation along the *z* axis direction and is generated using the pressure boundary condition in 3D (Zou and He, 1997). All other parameters are the same as given in the previous section. The simulation results are shown in Figure 3. The average velocity $\bar{u}=2.76\times10^{-4}$ was calculated using the velocity profile displayed in Figure 3. Substitution of the simulated average velocity into Equation (14) gives a value of *f*. Re = 56.82. This is in good agreement with the experimentally measured value of 57 (Tao and Xu, 2001).

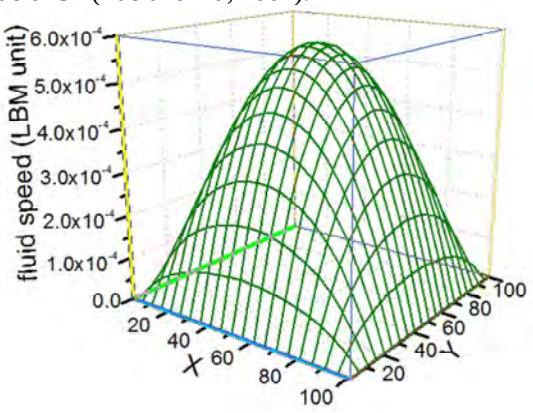


**Figure 3.** Fluid velocity profile of a cross section at *z*=25 in a rectangular duct.

A number of simulations have also been carried out by sub-dividing the flow region into multiple sub-regions. Different sub-regions have been assigned different constant values of $p_f$. The model is robust since it does not show any numerical abnormalities.

## SIMULATIONS IN REAL ROCKS

The present PP-LBM model is now applied to a real world tight-sandstone sample which consists of quartz, albite, calcite and pyrite. The cylindrical sample, which was drilled from Yaodian area of Yan'an in Erdors Basin, China, has a diameter and height of 3mm and 20mm respectively. The 3D microscopic distribution of mineral phases in the sample is generated with the in-house DCM software in a cubic region of 600 x 600 x 700 voxels (Li *et al.*, 2013). Each voxel represents a size of 3.7 x 3.7 x 3.7 $\mu m^3$. An arbitrary sub-domain of 200 x 200 x 50 voxels was selected for the following PP-LBM simulations.

In the sample, pyrite, quartz and albite particles are not permeable. Fluid can flow through void and the partially permeable calcite. Denoting the effective percolating fraction of calcite as $p_f^c$, the effective percolating fraction of a voxel is approximated as

$$p_f = v_o + p_f^c \cdot v_c \quad , \qquad (15)$$

where $v_o$ and $v_c$ denotes the volume fractions for pore and calcite in the voxel respectively.

The flow is driven by the same pressure difference as the rectangular duct simulation along the *z* axis direction. The pressure difference is implemented numerically in the same way which has been discussed in the previous section. All other parameters are the same as given in the previous section. Various values of $p_f^c$ from 0.0 to 0.2 have been used in the simulation. The typical velocity distributions in the simulated sample region are shown in Figure 4. As shown in Figure 4(a), the high-speed flow occurs only in small regions in the tight sandstone. By comparing Figure 4(b) with 4(c), it was found that just a small proportion of pores participated in the flow. Some pores effectively are not part of the flow path, as has been highlighted by the boxed regions in the figure. Most of the flowing path is occupied by calcite with a low flow speed. There are isolated relatively high-speed regions in the calcite. This indicates the existence of fine flow paths in these regions.

The same method is applied to a CIPS (Calcite In situ Preciptation System) core sandstone sample which consists of quartz and calcite. The 3D microscopic distribution of these mineral phases in this sample is generated with the DCM software in a cubic region of 1450 x 1470 x 340 voxels (Yang *et al*, 2012). Each voxel represents a size of 3.7 x 3.7 x 3.7 $\mu m^3$. An arbitrary sub-domain of 200 x 200 x 50 voxels is selected for the following PP-LBM simulations. The flow is driven by the same constant pressure difference as the tight-sandstone in the *z* axis direction and all the other parameters are the same as well. The same method as defined in Equation (15) is used to determine the effective percolating fractions.

In the LBM simulations, once flow is deemed to have reached steady state, the bulk permeability of the medium can be calculated, based on the generated velocity datasets, using Darcy's law as follows:

$$K = \frac{\nu \cdot < \rho u >}{\nabla P} \quad , \qquad (16)$$

where $K$ is the bulk permeability, $\nabla P$ is the pressure gradient in a particular direction, $\nu$ is the kinematic viscosity of the fluid and $u$ is the component of the velocity in the same direction as the pressure gradient. The quantity $< \rho \cdot u >$ is the average velocity flux over all the flow voxels taken directly from Equation (7).

The simulation is terminated once the following criterion has been reached:

$$\sum_t \frac{\|K(t) - K(t-1)\|}{\|K(t)\|} < 10^{-5} \quad . \qquad (17)$$

The convergence curves of the two samples are shown in Figure 5. The permeability of sandstone converges faster than tight sandstone. For sandstone, it requires 24000 time-steps to reach steady state, while it would need 162000 time-steps for tight sandstone. The code uses OpenMP to implement parallel computation to increase the calculating speed in C++ programs.

The calculated bulk permeability is shown in Figure 6. As anticipated, the bulk permeability increases with the effective percolating fractions of calcite. The bulk permeability of the tight-sandstone is more sensitive to the effective percolating fraction of calcite than for sandstone. That is, fine flow paths in calcite are more important for tight-sandstone than for sandstone. Flow in calcite phase in sandstone makes an insignificant contribution to the bulk permeability. The sandstone has a permeability value up to two orders of magnitude greater than the tight sandstone.

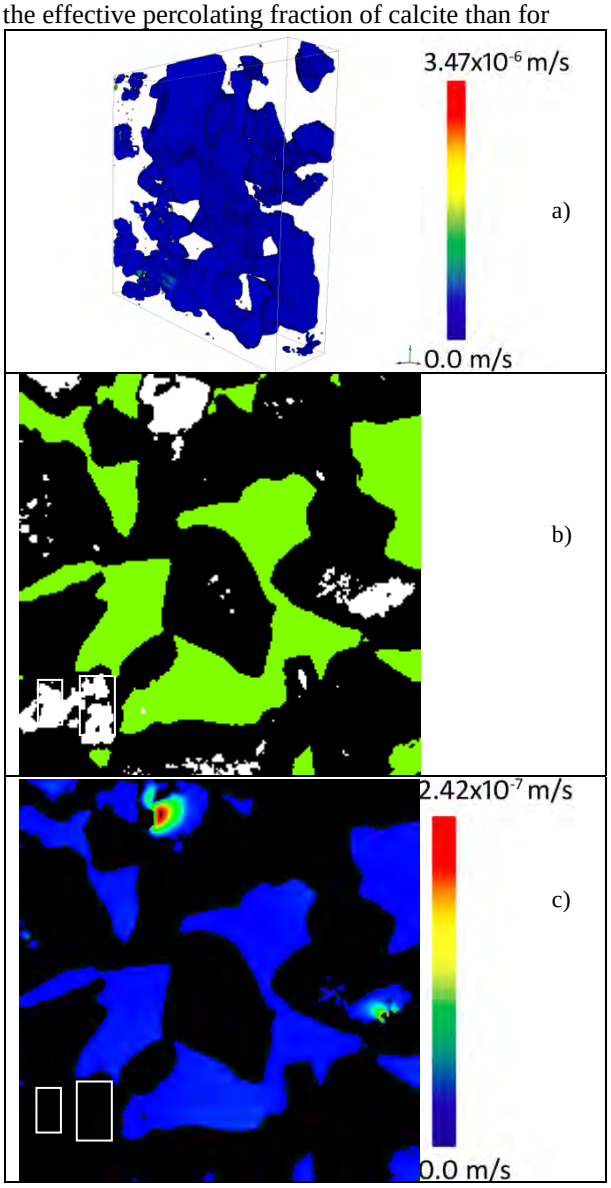


**Figure 4.** Velocity distribution of a tight sandstone sample where the non-percolating regions voxels are displayed as white and the percolating fraction of calcite is 0.2. (a) 3D velocity distribution image. The high flow speed region is small so it is not visible clearly on the figure. (b) Microstructure composition distribution at slice 20 with pore, calcite and mixture of quartz, albite and pyrite represented by white, green and black. (c) Velocity distribution at slice 20.

In relation to bulk permeability, flow in the calcite phase is essential for tight-sandstone, whereas it could be neglected for sandstone.

## CONCLUSIONS

A partially percolating lattice Boltzmann model (PP-LBM) defined on partial volume voxels, rather than binary voxels, is developed. An effective percolating fraction is introduced on each voxel to incorporate the partial volume effect into the partial-bounce-back LBM model. The partial volume effect is related to the fine structures which are smaller than the voxel size, which can be characterized using DCM. The effective percolating fractions of voxels were estimated using the DCM generated volume factions. The PP-LBM is implemented numerically on the square lattice in 2D with square pixels and on the simple cubic lattice in 3D with cubic voxels. In relation to fluid flow, each voxel (pixel) is defined by an effective percolating fraction $p_f$ which is related to the voxel (pixel) permeability, compositional volume fractions and sub-voxel (sub-pixel) fine structures. Fluid flows on regular geometries in 2- and 3-dimentions have been simulated. The numerical results agree with known analytic solutions.

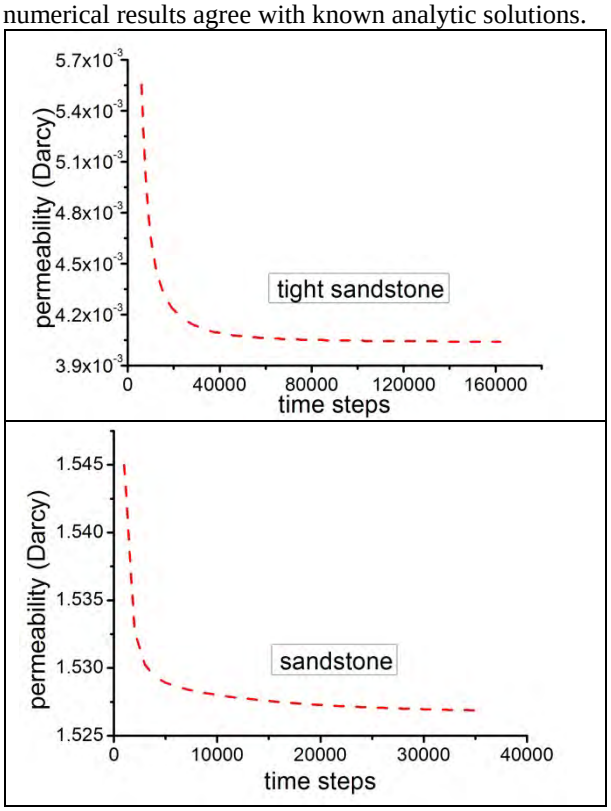


**Figure 5.** Convergence lines of permeability for tight sandstone and sandstone. The percolating fraction of calcite is 0.0.

The PP-LBM approach has been used to simulate flow in two real-world rock samples – a tight-sandstone and a CIPS sandstone. With the CIPS sandstone, the bulk permeability is insensitive to flow in the calcite phase. Therefore, the conventional LBM flow simulations on image-segmented X-ray CT images would be adequate. However, with the tight-sandstone, the numerical results indicate that the fine flow paths in the calcite phase play a critical role. When the flow paths in the calcite phase are neglected, the sample is essentially non-permeable. That is, the conventional LBM simulation on image-segmented X-ray CT images would produce misleading results. The tight oil & gas resources are going to play an increasingly important role for sustainable energy supply in the world. The PP-LBM and DCM would be useful tools for characterization and modeling of the tight reservoirs.

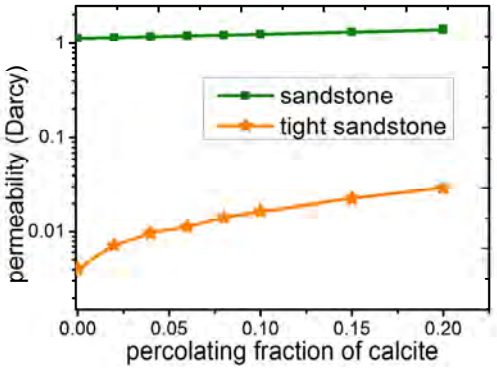


**Figure 6.** Effect of different percolating fractions of calcite on bulk permeability.

The PP-LBM approach is generic and should be applicable to other types of unconventional reservoirs and advanced materials. Work along this line is in progress.

## REFERENCES

BALASUBRAMANIAM, K., HAYOT, F. and SAAM,W.F., (1987) "Darcy's law from lattice- gas hydrodynamics", *Phys. Rev. A*, **36**, 2248–2253.

CHEN, Y. and ZHU, K., (2008) "A study of the upper limit of solid scatters density for gray Lattice Boltzmann Method", *Acta Mech. Sin.*, **24**, 515–522.

DARDIS, O. and McCLOSKEY, J., (1998a) "Lattice Boltzmann scheme with real numbered solid density for the simulation of flow in porous media", *Phys. Rev. E*, **57**, 4834–4837.

DARDIS, O. and McCLOSKEY, J., (1998b) "Permeability porosity relationships from numerical simulations of fluid flow", *Geophys. Res. Letts.*, **25**, 1471–1474.

DESRUES, J., VIGGIANI, G. and BESEUELLE, P. (eds) (2006) "Advances in X-Ray Tomography for Geomaterials", (London: ISTE)

GAO, Y. and SHARMA, M.M., (1994) "A LGA model for fluid flow in heterogeneous porous media", *Transp. in Por. Media*, **17**, 1–17.

HECHT, M. and HARTING, J., (2010), "Implementation of on-site velocity boundary conditions for D3Q19 lattice Boltzmann simulations, J. of Stat. Mech.: Theory and Exp. (http://iopscience.iop.org/1742-5468/2010/01/P01018)

LI, R.R., KONG, H., YANG, S., MAYO, S., ZHU, R., BAI, B., PAN, J. and WANG, H., (2013) *CSIRO Data Collection: Erdors Basin Yanchang Formation Tight Sandstone 3D Microstructures*

PEREIRA, G.G., DUPUY, P.M., CLEARY, P.W., DELANEY, G.W., (2012), "Comparison of permeability of model porous media", *Prog. in Comput. Fluid Dyn.*, **12**, 176-186.

TAO, J., and XU, J., (2001), "The fluid flow rule at laminar flow in rectangle shape channel", *Journal of Huainan Institute of Technology*, **2**,1-10.

THORNE, D. and SUKOP, M., (2004) "Lattice Boltzmann model for the Elder problem" In: Proceedings of the XVth International Conference on Computational Methods in Water Resources (CMWR XV), Chapel Hill, NC, USA, June 13–17. Elsevier, Amsterdam, 2004, pp. 1549–1557

WALSH, S.D.C., BURWINKLE, H. and SAAR, M.O., (2009) "A new partial-bounce back lattice-Boltzmann method for fluid flow through heterogeneous media", *Computers & Geosciences*, **35**, 1186–1193.

YANG, Y.S., TULLOH, A., COLE, I., FURMAN, S. and HUGHES, A., (2007) "A data-constrained computational model for morphology structures", *J. Aust. Ceram. Soc.*, **43**, 159–164.

YANG, Y.S, FURMAN, S and TULLOH, A. "A data-constrained 3D Model for material compositional microstructures", *Adv. Mat. Res.*, **32**, 267-270.

YANG, S, LIU, K, MAYO, S, and TULLOH, A, (2012) *CSIRO Data Collection: CIPS sandstone microstructure*

ZHU, J. and MA, J.S., (2013) "An improved gray lattice Boltzmann model for simulating fluid flow in multi-scale porous media", Adv. in Water Res., **56**, 61–76.

ZOU, Q and HE, H., (1997) "On pressure and velocity boundary conditions for the lattice Boltzmann BGK model", *Phys. Fluids*, **9**, 1591-1598.